High-resolution measurements of pressure solution creep

Dag Kristian Dysthe,* Francois Renard,† Jens Feder, Bjørn Jamtveit, Paul Meakin,‡ and Torstein Jøssang
Physics of Geological Processes, P.O. Box 1048, Blindern, N-0316 Oslo, Norway
(Received 27 July 2002; revised manuscript received 3 March 2003; published 14 July 2003)

Two dilatometers with high precision and stability have been developed for measurement of indentation by pressure solution creep. The indentation of gold wires or glass cylinders into sodium chloride has been measured with down to 10 Å accuracy and 6% precision. The indentation curves show a strong history dependence and the indentation rate decreases by three orders of magnitude over 400 h. The indentation mechanism is shown to be a pressure solution creep process in which material is dissolved at the indentor-sodium chloride contacts and transported to the free surface, where it precipitates in the proximity of the indentors. The indentation rates are not controlled by precipitation rates, the density of preexisting dislocations in the material, by change in the contact widths, or by ordinary plastic deformation. Small amplitude sinusoidal variations of temperature and normal stress are shown to have a large effect on the indentation rate. Moreover, sudden increase in normal stress from the indentor on the sodium chloride is shown to initiate an increased, time-dependent indentation rate. A model for pressure solution creep with time-dependent contact sizes explains the history dependence of the indentation data presented.

DOI: 10.1103/PhysRevE.68.011603 PACS number(s): 68.08.−p, 68.15.+e, 68.37.−d, 68.55.−a

I. INTRODUCTION

Adhesion and friction between two rigid bodies depend on the area of contact. To obtain a large area of contact between two rigid bodies normally requires deformation or creep in the region close to the contact. When stresses in the contact region are too small to activate dislocation motion, mass transport in a surrounding fluid phase, so called pressure solution creep (PSC), is the most efficient creep mechanism. As a low temperature analog to Coble creep, PSC is important in transforming loose sediments to sedimentary rocks with tensile strength (adhesion at contacts). This is a striking example of strain hardening. During PSC, stress concentration at the grain contacts causes local dissolution, diffusion of the dissolved material out of the interface region and deposition on the less stressed surfaces of the grains [1]. PSC plays a major role in controlling the plasticity of the earth's crust during compaction of sedimentary basins [2] and during tectonic deformation [3]. It is also responsible for the strengthening of the gouge in active faults following earthquakes [4,5]. PSC is also important in ceramic processing [6]. Despite the importance of PSC in a number of areas of science and technology, and the interesting fundamental character of this surface controlled, mechanochemical, strain hardening deformation process, it has received little attention from physicists.

A simple theoretical description of the PSC is required as a background for discussing the exacting requirements for experiments on PSC and the significance of the results presented here. We do not discuss the details that separate earlier descriptions [1,7,8], but emphasize their common elements.

In the main part of this paper, we describe in detail two high-resolution dilatometers for single contact PSC experiments. We verify that the accuracy and precision necessary for detailed, quantitative studies of single grain contacts under PSC have been achieved, and we then present results that cast new light on the history dependence of PSC.

A. Current models of pressure solution creep

Our discussion of PSC is focused on the behavior of an inert indentor that is pushed into a soluble mineral in the presence of a reactive solution. The development of a better understanding of the behavior of compacting aggregates in terms of such simple systems entails many assumptions that are not the subject of this study.

In a system like that illustrated in Fig. 1(a), an inert indentor of dimension d_i is pressed with a constant force F into a soluble solid surface immersed in a solvent which is at equilibrium with the unstressed solid. In general, there are a number of contact areas of mean dimension d_c. The distance between the surface of the indentor and the dissolving solid is Δ_c in the contact areas, and Δ_i is the mean separation over the entire indentor contact region. The contact region (microscopic or macroscopic) is represented in Fig. 1(b). In this case, the solid materials are separated by a fluid filled gap with thickness of Δ and a lateral dimension of d. We are interested in the vertical displacement of the indentor z or the indentation rate $\partial z/\partial t$.

The driving force for pressure dissolution is the variation in chemical potential μ along the surface of the soluble solid. The gradient in chemical potential is assumed to be proportional to the gradient in normal stress on the surface, $\partial\mu/\partial r \propto \sigma_n/d$, where $\sigma_n=(F/d_i^2-p_f)$ and F is the force acting parallel to z on the indentor and p_f is the fluid pressure [7,8]. If the rate limiting step in the process is dissolution, the rate of indentation $\partial z/\partial t$ is proportional to σ_n and $\partial z/\partial t$ is independent of d and Δ.

If the rate limiting step in the process is transported from the stressed to the unstressed area of the surface, we have to

*Electronic address: d.k.dysthe@fys.uio.no
†Present address: LGIT-CNRS-Observatoire, Université Joseph Fourier, Grenoble F-38041, France.
‡Present address: Idaho National Engineering and Environmental Laboratory, P.O. Box 2209, Idaho Falls, Idaho 83415-2209, USA.

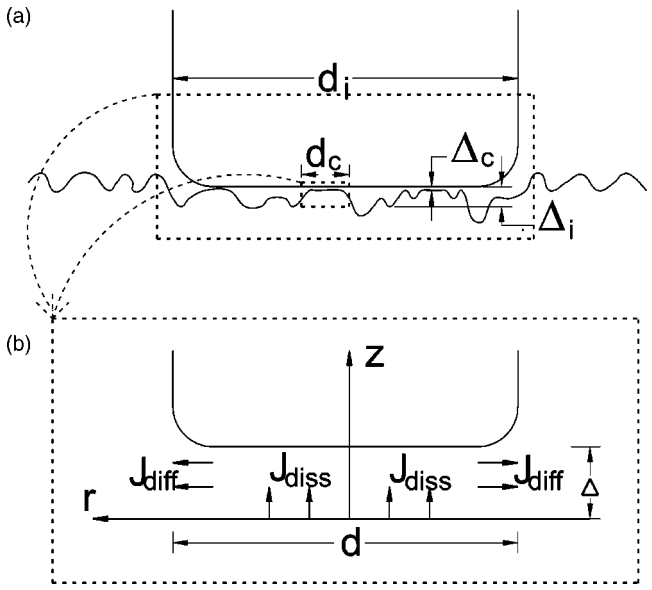

FIG. 1. Simplified model of an indentor on a pressure dissolving surface. (a) An indentor of width d_i is pressed against a soluble surface. The indentor is in contact with the surface in several discrete regions with dimensions of the order of d_c. On both the indentor scale and the contact scale, the contact region may be decribed by the model illustrated in (b). In the contact region of dimension d, a normal stress causes a dissolution flux J_{diss} from the soluble surface into the fluid region of width Δ. This material is transported by a diffusive flux J_{diff} out of the contact region.

consider the dimensions of the indentor and the contacts. The analyses in Refs. [1,7,8] indicate that

$$J_{\mathrm{diss}}\pi r^2 = J_{\mathrm{diff}} 2\pi r\Delta = -2\pi r\Delta L\frac{\partial\mu}{\partial r}, \tag{1}$$

where J_{diss} is the flux of dissolved material on the solid surface, J_{diff} is the flux of dissolved material through the contact region aperture of width Δ, and L is a phenomenological transport coefficient which is proportional to the diffusion coefficient D. The indentation rate is proportional to the dissolution flux:

$$\frac{\partial z}{\partial t}\propto J_{\mathrm{diss}}\propto\frac{\Delta D}{d}\frac{\partial\mu}{\partial r}\propto\frac{\Delta D\sigma_n}{d^2}. \tag{2}$$

Equation (2) for the indentation rate may be used on two different length scales, the indentor and the contact length scales (see Fig. 1). On the indentor scale, the transport thickness Δ may be either the thickness of a fluid film between the solid surfaces as proposed by Weyl [1] (the fluid film model) or the effective cross section of a fluid channel network in an island-channel network as proposed by Raj and Chyung [8] (the island-channel model). In the fluid film (FF) model, the thickness Δ is of the order of 1–10 nm and the diffusion coefficient is the same as or up to an order of magnitude lower than the bulk diffusion coefficient [9]. Thus, in the FF model, 10^{-19} m^3/s$<\Delta D<10^{-17}$ m^3/s at room temperature and moderate normal stresses (<10 MPa).

In the island-channel (IC) model, Δ is of the order 0.1–1 μm and the diffusion coefficient is the same as the bulk value, thus 10^{-16} m^3/s$<\Delta D<10^{-15}$ m^3/s at room temperature, and the compaction rate estimated for the IC model is larger by a factor of 1–4 orders of magnitude than the rate estimated for the FF model.

It has been proposed [10,11] that the rate limiting step in an island channel model is the transport of dissolved solid out of each contact region (in the island regions) and in each contact region the solid surfaces are separated by a thin fluid film. This implies that the contact regions are the same in the IC and the FF models and they can be characterized by the same variables Δ and D. We will refer to this model as the island fluid film (IFF) model. Attempts have recently been made to theoretically estimate the characteristic contact size d_c [12,13], and various observations give the range 10^{-7} m $\leqslant d_c \leqslant d$. Thus, the indentation rates $\partial z/\partial t$ for the IFF model lie between those of the IC and the FF models. In all these models, all the parameters are considered to be constant (it is assumed that the system is in a steady state). In other words, *there is no history dependence* or strain hardening in the current models of indentation by PSC.

B. Previous experiments

PSC is a slow process, and this must be taken into account in the design of experiments. Dissolution rates normal to the contact surface of a single contact undergoing PSC are of the order of $\approx 10^{-6}$ m/day for sodium chloride, $\approx 10^{-9}$ m/day for calcite, and $\approx 10^{-12}$ m/day for quartz [14]. In earlier experiments, the basic strategy was to measure PSC over a long period of time, and multiply the number of grain-grain contacts by performing measurements on aggregates (dense grain packings in confined regions), or to measure very small displacements.

1. Aggregate experiments

Large amounts of data on compaction of aggregates have been valuable in establishing the dependence of PSC on temperature, stress, mineralogy, and grain size. The influences of fluid chemistry and clay content have also been quantified to some extent [15]. The main problem with aggregate experiments as performed until now is the difficulty in interpreting the data. The effects of complex aggregate geometry and dynamics, increasing contact areas and grain scale dynamics cannot be individually resolved. The interpretation of the experiments must rely on previously established models, and the experiments are not designed to test the models.

2. Single contact experiments

A number of experiments have cast light on the fundamental principles of PSC at the grain-grain contact scale. Sprunt and Nur [16] and later Brok and Morel [17] studied the effect of elastic strain on the dissolution of minerals, and Tada and Siever [18] showed in qualitative experiments that plastic strain in the grain-grain contact region may be fundamentally important.

Spiers and co-workers [19–22] have performed an impressive series of experiments focused on the microstructure

at the grain-grain contacts. In these studies, aggregates compacted by PSC were studied *ex situ* by electron microscopy revealing an ''island-channel'' structure. *In situ* imaging of single contacts revealed the first qualitative evidence for these island-channel structures, and indicated how they evolve with time [22].

Hickman and Evans [23,24] imaged salt lenses pressed against windows in the presence of brine. They used the movement of Newton rings to measure the convergence of the lens and the window. When an inert glass window was used, they measured convergence rates with 40% repeatability (three experiments). They could not resolve any dependence on stress when the stress was varied by a factor of 10. When windows formed from the same salt as the lens were used, they observed precipitation around the contact and no convergence. These experiments initiated a debate on the relative importance of contact healing and PSC during the compaction of aggregates.

PSC is a process that involves dissolution, transport, and precipitation at *constant overall fluid saturation*. The only concentration gradients in the fluid should be caused by stress on the mineral surface. Since mineral solubility is, in general, a function of temperature it is necessary to have a *very small fluid volume* with *minimal spatial or temporal variations in temperature*. It is also necessary to verify that the mass balance of dissolved and precipitated material is satisfied. All experiments to date used fluid volumes of 1 ml or more, no control over where dissolved matter precipitated and temperature fluctuations of the order of 0.1–1 K.

If the measurement of the time (history) dependence of the PSC rate is required, both high resolution and good stability of the measurement device over the duration of the experiment are essential. Published experiments had height resolutions down to 0.1 μm, except that of Hickman and Evans [23,24] for which a resolution of 0.01 μm was claimed. The long time stability of the measurement devices are normally not reported in detail, but can be assumed to be of the order of ten times the resolution.

II. EXPERIMENTAL TECHNIQUES

We use two different capacitance dilatometers in this study, a single capacitance dilatometer built for long time stability and high accuracy and a differential dilatometer built for measurement of short time response to temperature and stress changes. The single capacitance dilatometer has previously been used with dry samples and has been described before [25]. However, we describe the instrument in some depth because several modifications have been carried out to study PSC with the necessary accuracy and precision.

A. Measurement principle

Figure 2 shows the principle of the capacitance dilatometer that was used in this study. At the bottom of the sample holder (a hollow quartz cylinder glued to a sapphire window) indentors (gold wires) were placed and a few microlitres of water were added. On top of this, a small single crystal of soluble material with a diameter of $\approx$5 mm was placed and a fluid that is immiscible with water (hexadecane) was added

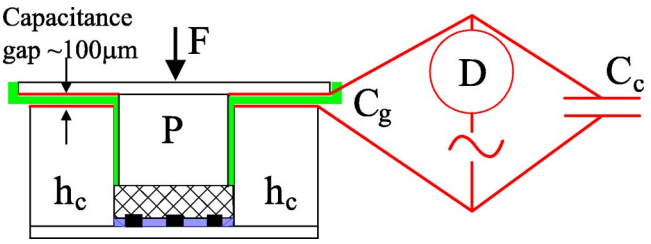

FIG. 2. Schematic diagram of the capacitance dilatometer. The sodium chloride single crystal (hatched rectangle) sits inside a hollow cylinder (hc) that is glued onto a sapphire window. The indentors (black rectangles) that are pressed onto the sample by a piston *P* lies on top of the crystal. A flat quartz plate coated on one side with gold to produce an electrically conducting surface is placed on top of the piston. A small volume of saturated brine that is inhibited from evaporating by hexadecane lies in the contact between the indentor(s) and the salt crystal. The top of the hollow cylinder is electrically conducting so that the $\sim$100-μm-wide gap between hc and the flat gold-coated quartz plate on top forms a capacitor. The capacitance C_g of the gap is inversely proportional to the thickness of the gap. This capacitance can be measured by an impedance analyzer or by measuring the imbalance in a bridge with a constant, known capacitance C_c. The force F applied on the top of the assembly causes the indentors to penetrate into the crystal by PSC, and the indentation distance is inversely proportional to the change in capacitance.

to isolate the brine volume from the atmosphere. On top of the crystal, a piston ground to a height at which the top surface reached 50–100 μm above the surface of the hollow cylinder was placed and a quartz plate was placed on top of the piston. The bottom surface of the quartz plate and the top surface of the hollow cylinder were coated with gold that was electrically connected to either an impedance analyzer or a capacitance bridge with a lock-in amplifier (as shown in Fig. 2) for measuring the capacitance of the gap C_g. The capacitance C_g is inversely proportional to the width d of the gap:

$$C_g = \frac{\varepsilon_0 \varepsilon_r \pi (r_o^2 - r_i^2)}{d}, \tag{3}$$

where ε_0 is the permittivity of vacuum, ε_r is the relative permittivity of hexadecane and r_i and r_o are the inner and outer radii of the electrodes, respectively. The force F applied on the top causes the indentors to penetrate into the crystal by PSC, and the indentation distance is inversely proportional to the change in capacitance.

B. Single capacitance dilatometer

1. Indentor geometries

Several indentor types and geometries were tried. These included 0.1-mm-diameter glass beads, gold and steel wire mesh, electron microscope grids, glass lenses, optical fibers, and gold wires. The indentors should be inert and have a known shape to allow the contact area to be calculated as a function of indentation. The identors should also cover a sufficiently large area to average over local heterogeneities in

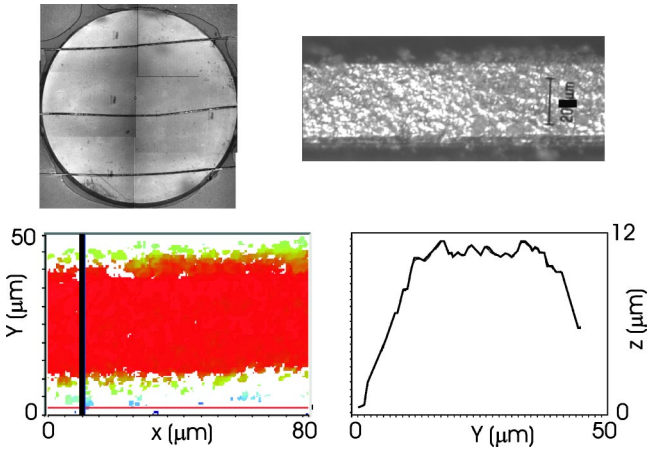

FIG. 3. Indentor geometry in the gold wire cell. Upper left: A picture taken through the bottom of the cell showing a crystal sitting on three gold wires. Upper right: Microscope picture of gold wire surface roughness. Lower left: White light interferometer picture of gold wire profile. Lower right: Measured gold wire profile from image on lower left.

the crystal surface yet have small enough dimensions to allow rapid diffusion of material out of the contact area and maintain mechanical stability. We found that gold wires that were pressed flat fulfilled these conditions. For stability we used three gold wires. Figure 3 shows a picture of gold wires in the sample cell viewed through the sapphire glass bottom. It also shows white light interferograms of a gold wire profile and the surface structure of a gold wire. A gold wire profile from the interferogram that shows the average form and dimensions is also included in the figure. Although the contact area between gold wires and NaCl surface is not constant, the change in contact area with indentation and its effect on the PSC rate is modeled and compared to experimental data (see Fig. 8).

2. Thermal stability

Temperature has to be controlled very accurately to avoid thermal dilatation and changes in the solubility of the sample. To achieve this we have used a three stage thermal control. The room temperature was controlled to ± 1 K by an air conditioning unit. This ensures small variations in temperature for the electronic equipment, and a first stage in controlling the temperature of the sample. The principle of the next two stages of the thermal control system is illustrated in Fig 1 of Ref. [26]. Oil is circulated through a copper enclosure that surrounds the inner part of the apparatus. The oil temperature is controlled by a control loop consisting of a temperature sensor and a heating element in a circulation bath on a refrigerating element. Before it reaches the copper enclosure, the oil flowing from this temperature control unit is passed through a low pass filter designed to remove fluctuations generated when the heating element turns on and off. The oil tubes and copper enclosure are insulated from the air in the room. Using only the air condition and the oil circulation system, the temperature in the sample holder is kept constant with a standard deviation of 20 mK. Inside the

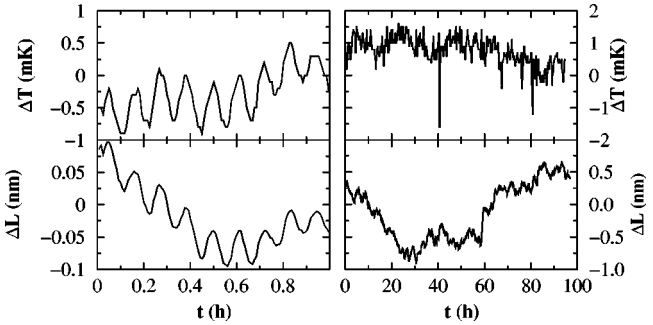

FIG. 4. Thermal stability, measurement resolution, and measurement stability. Left hand side: measurement of temperature (top) and dilatation of a copper test sample (bottom) when the proportional-integral-derivative (PID) control is used to modulate the temperature with an amplitude of 0.5 mK. Right hand side: measurement of temperature (top) and dilatation (bottom) of an inert quartz glass sample over a long time period.

copper enclosure, the inner copper block is in good thermal contact with the enclosure only through a Peltier element. On the top surface of the Peltier element is a thermistor that is used in a control loop (proportional-integral-differential (PID) control) with the Peltier element to modulate heat flow into the inner copper block. The inner copper block has a large thermal mass compared with that of the sample holder. Good thermal contact of the sample with the copper block is ensured by using a sapphire flat as the base of the sample holder (sapphire has a thermal conductivity 40 times the thermal conductivity of glass). The temperature measurements were performed using a quartz thermometer in the copper block close to the sample holder. Due to the small sample and fluid volume with respect to the copper volume, we assume that thermal gradients in the sample and fluid are of the same order of magnitude as or smaller than the measured short time thermal fluctuations.

The thermal response function of the system has been well studied and described [25]. We have performed recalibrations with the current sample holder and improved the long time thermal stability. Typical results are displayed in Fig. 4. The left hand side shows the measurement of temperature and dilatation of a 5-mm-high copper sample when the PID control is used to modulate the temperature with an amplitude of 0.5 mK. Using this ac technique, a corresponding thermal expansion of the copper sample of 0.4 ± 0.05 Å was measured. On the right hand side, measurements of the temperature and dilatation of a quartz glass sample, over a long period of time, are shown. The temperature has a standard deviation of 0.5 mK.

3. Mechanical and electrical stability

An instrument to measure small displacements must be mechanically stable and frictionless [27]. The principle used in this instrument is simply to place the components on top of each other in a ''pile'' that does not need side walls for stability. This requires that all of the surfaces must be parallel and all of the components must be axially symmetric. When we tried to use the walls to stabilize a similar assembly, the measured elastic response to the load change (nomi-

nally a few nanometers) was completely dominated by friction. The transmission of force from the dead weight to the upper plate of the capacitor is not friction free in this setup, but thermal dilatation experiments show no hysteresis, and we conclude that the small friction in this part is not important.

Great care has also been taken to achieve electrical stability. Deterioration of contacts and solder joints over period of weeks may make accurate measurements impossible. Adequate screening of signal leads to minimize the effects of noise and ground loop currents and is essential. Even turning on the lights in the laboratory induced currents that were sufficient to overload the detector. The most difficult problem was to keep water from creeping out of the sample holder and into the capacitance gap. This was finally achieved by silanating the quartz glass hollow cylinder and piston with a solution of chlorotrimetylsilane in toluene for 15 min and drying at 150 °C. In addition, the sample holder and capacitance gap were filled with hexadecane, which has a relative permittivity of 2.0 under ambient conditions. The right hand side of Fig. 4 shows measurements of the temperature and dilatation of a quartz glass sample over a long period of time. Since the quartz glass sample is made of the same material as the hollow cylinder, there should be no differential dilatation if the temperature fluctuates. The measurement therefore reflects the long time stability of the electronic circuits and the mechanical components. Quartz glass hollow cylinders were used in this experiment because of the low thermal expansion coefficient of quartz. The dilatation measurement has a standard deviation of 4 Å. The electrical and mechanical stability of the instrument is therefore estimated to be better than 10 Å over a month.

C. Differential dilatometer

The differential dilatometer is shown in Fig. 1 of Ref. [26]. The symmetrical design with two, nominally equal capacitances, pistons and samples, one wet and one dry, is chosen to cancel out all effects but those caused by differences on the two sides (presence or absence of water). The dilatometer is designed to allow inspection by microscope. The presence of a microscope objective close to the sample limits the available space and the possibility of an extreme thermal control and long time stability as in the single capacitance dilatometer.

The outer part of the instrument consists of an isolated brass block with tubes spiraling down the outer perimeter. Thermostated water is flowed through these tubes as the first step in the thermal control. Heat flow from the outer brass block to the inner aluminum block is transmitted through Peltier elements. The heat flow is modulated by controlling the current through the Peltier elements. This is performed in a PID control loop with the temperature measurement from a thermistor in the aluminum block as the control variable. It is preferable to use materials with a small thermal expansivity in the dilatometer, but since this is a differential design we chose to depart from this principle. Aluminum has been chosen for the inner block and the electrodes because they can be eloxated to obtain an electrically isolating layer of aluminum oxide. This makes it much easier to pass the thin electric leads to the electrodes without short circuiting.

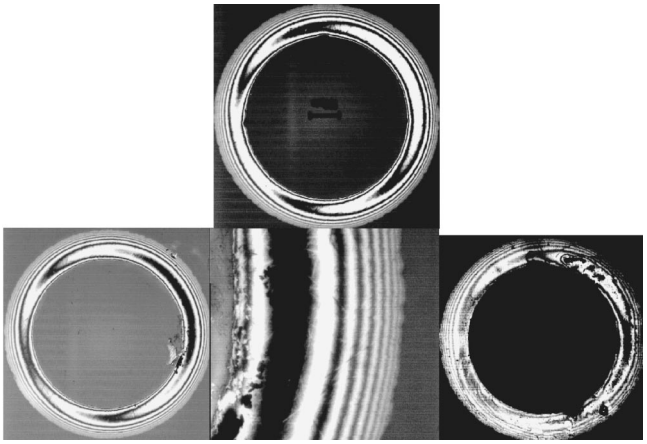

FIG. 5. Microscope view of contact surface between sodium chloride sample and tripod. Interference fringes from green light (550 nm) show that the maximum distance between the surfaces of the capillary tubes and the sodium chloride surface is 2 μm.

The electronic circuit is a specialized lock-in amplifier built in-house based on that of Jones [27]. Compared to the single capacitance in Fig. 2, the main difference is that the balancing capacitance C_c is now mechanically and thermally almost identical to the measuring capacitance.

A tripod construction is chosen for stability. It is made of a quartz glass cylinder of 5 mm diameter and ≈ 2 mm height with three cylindrical legs. The legs, glass capillary tubes of outer diameter 1 mm, inner diameter 0.8 mm, and height ≈ 1 mm, are glued with a very thin layer of light curing glue to one of the flat surfaces of the quartz glass cylinder such that all four cylinder-tube axes are parallel. The lower surfaces of the three glass tubes are carefully ground flat and parallel to the quartz glass surfaces. Figure 5 shows the microscope view of the contact surface between a sodium chloride sample and the three legs of the tripod before any indentation has taken place. Interference fringes from green light (550 nm) show that the maximum distance between the surfaces of the capillary tubes and the sodium chloride surface is 2 μm.

Figure 6 shows measurements with the differential dilatometer of temperature and dilatation over a period of 20 h. In this experiment both sides of the dilatometer were dry, but otherwise as shown in Fig. 1 of Ref. [26]. The temperature has a standard deviation of 5 mK. The temperature fluctuations are ten times larger than in the single capacitance dilatometer, but still small enough to have a negligible effect on the PSC. There is a measured indentation rate of 0.3 to 1 nm/h that is in part due to plastic creep in asperities in the contact and in part due to electrical noise. The slow drift is nearly three orders of magnitude smaller than the indentation rates by PSC (see below) and therefore negligible. The sudden change in measured indentation illustrates the magnitude and time scale of electrical noise that affects the measurements. Such disturbances are often easy to detect as noise, but not always.

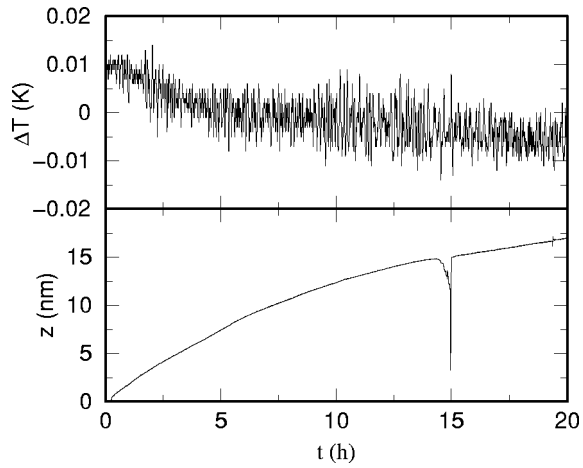

FIG. 6. Stability of temperature and differential dilatometer with tripod and dry sodium chloride at 0.8 MPa on both sides. The drift of the dilatometer at start of experiment is 1 nm/h and decreasing to 0.3 nm/h after 20 h is probably due to plastic creep at the very small contact points. The disturbance at 15 h is a typical problem, this one occurring at 8 in the morning when electric machinery is switched on. The exact cause is unknown.

III. RESULTS

All the results presented here were obtained using sodium chloride at room temperature. To avoid the important problem of dissolution vs establishment of a solid, nondissolving interface [24,22] leading to contact healing, we used inert indentors on the sodium chloride surfaces.

A. Indentation of sodium chloride by plasticity

Sodium chloride has a hardness of 2–2.5 on Mohs' scale [28]. The plasticity of sodium chloride has raised some concern that it is not a good analog material for PSC experiments, but comparison with PSC in sodium chlorate which does not deform plastically at room temperature shows that plasticity does not play a key role in PSC of sodium chloride [29]. However, we have performed some experiments to quantify the effect of plasticity in our setup. A single sodium chloride crystal with ground surfaces was dried with a flow of pure nitrogen gas for 2 min and placed on gold wires in our experimental cell and covered by hexadecane. The crystal was put under constant loads corresponding to stresses of 2, 7, 12, and 17 MPa. The normal stresses were calculated by measuring the areas of contact determined from the imprints of the gold wires on the sodium chloride surfaces, after the experiment was completed. The imprint corresponds to the area of contact after the highest load. Figure 7 shows the details of one such imprint. Grooves from the grinding process can be seen running in all directions and the 20-μm-wide groove imprinted by the gold wire, which runs horizontally in the picture, can also be seen. Since the imprint is at least as large as the maximum contact area, it might be expected that the real area of contact for the initial (smallest) load was smaller. The estimated normal stress of 2 MPa is therefore a lower bound. In a later experiment using a 4 MPa normal stress, we were not able to identify the

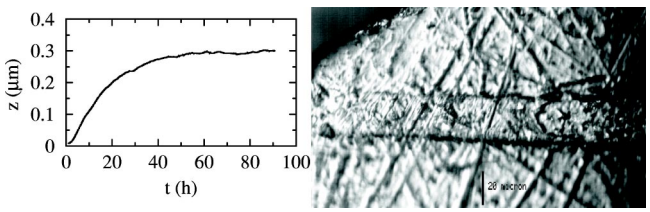

FIG. 7. Indentation of gold wires in sodium chloride by plastic deformation. Top: Indentation vs time with nominal load of 4 MPa. Bottom: microscope picture of surface deformation with 17 MPa normal stress.

imprints in the crystal when the surface was inspected with a microscope. Figure 7 shows the displacement creep for dry, plastic deformation with a (nominal) load of 4 MPa. The total creep over 100 h is smaller than the average roughness of the crystal surface. The mean creep rate during the last 50 h was 0.2 nm/h. Since no process other than plastic creep contributes to smoothening of the interface between the gold wires and the crystal, the creep shown in Fig. 7 is an upper bound for the contribution of plastic deformation to the PSC measurements presented below.

B. Indentation of sodium chloride by pressure solution

A series of experiments were carried out in which gold wires indented sodium chloride in the presence of saturated brine. The experimental results are shown in Fig. 8. The only treatment of the raw data before presenting them in Fig. 8 was conversion of capacitances to gap heights and subtraction of the initial gap heights (that varied between 50 and 200 μm from experiment to experiment).

The most striking feature of the indentation curves in Fig. 8 is the rapid initial indentation (up to 2 μm/h) and continuous decrease in the indentation rate (to about 2 nm/h at 370 h). This behavior appears, at first sight, to be similar to logarithmic creep caused by exhaustion of moving dislocations [30]. However, a more detailed examination of the data indicates that these cannot be well represented by a logarithmic form. We will return to possible explanations of these results in the discussion.

The indentation rate during the first 10 h varied greatly between the different experiments, but after 10 h all the curves behaved very similarly. We believe that this is due to the dissolution of contacts caused by initial surface roughness, deviations from flatness, and mismatch of the two surfaces. After $\approx 1-12$ h, the three gold wires have established contact along the entire length of the wires, and the roughness from grinding, polishing, or cleaving has been dissolved away. This has been confirmed by measuring the depth of the dissolution grooves and comparing it with the measured total indentation in each experiment. A further indication that all the experiments have reached a similar stage after about 10 h is that the indentation rates (slopes of the curves in Fig. 8) are similar, varying from 110–220 nm/h with a mean of 170 nm/h and a standard deviation of 50 nm/h. Consequently, in the lower graph of Fig. 8, we have shifted the experimental curves vertically to coincide at $t=10$ h. This graph ilustrates the extremely good repeatability of the experiments. At t

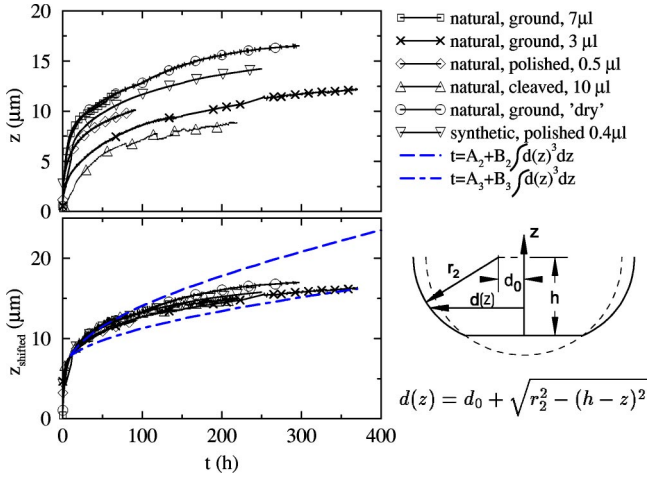

FIG. 8. Indentation of gold wires in sodium chloride by PSC at 4 MPa normal stress and ambient temperature. Upper graph: Experimental indentation curves for natural and synthetic sodium chloride with ground, polished, and cleaved surfaces and varying amounts of brine. The ''dry'' experiment shows, as explained in the text, PSC with only an adsorbed layer of water on the NaCl surface. Symbols on curves every 500–1000 data points. Lower graph: Experimental curves shown above, shifted to coincide at $t=10$ h. Model curves (long dashed and dash-dotted) represent the effect of only changing contact area of gold wire according to the model for the gold wire cross sections shown in the lower right corner.

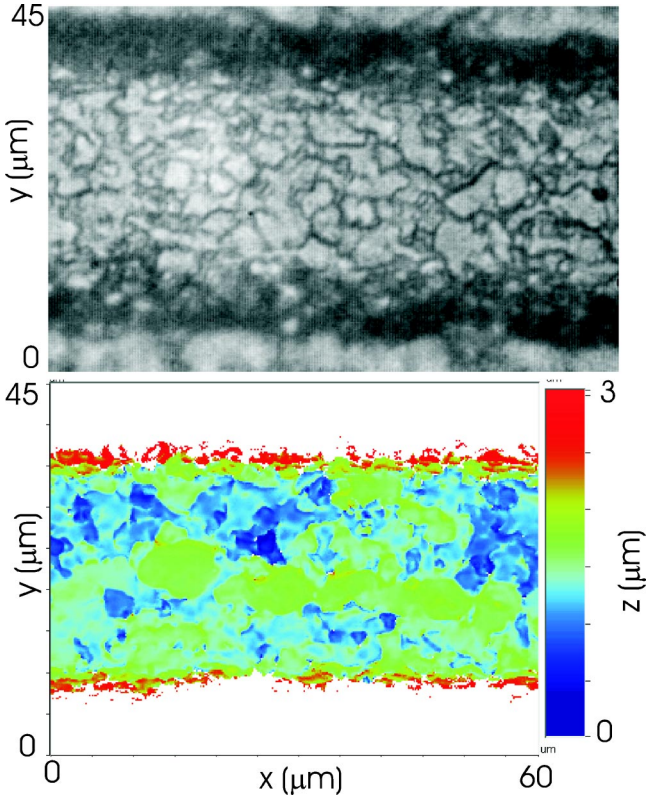

FIG. 9. Structure of the contact region after indentation by PSC. Optical micrograph (top) and white light interferometer image (bottom) of groove indented by PSC. Shell-like or island-channel-like structure with plateaus of linear dimension 2–6 μm, shallow channels (≈ 1 μm) and deep pits (≈ 3 μm) in between. This type of structure was generic to these experiments with small variations due to original surface treatment of the crystal and duration of the experiment.

$=200$ h, the standard deviation is 5% in z and 9% in $\partial z/\partial t$.

The experiments were performed with the same cell (using gold wires) and normal force as the plastic deformation experiment (see Fig. 7). The indentations after 100 h were 25–50 times larger with brine present. The rate of indentation after 100 h was 27 ± 1 nm/h for all the wet experiments, more than 100 times larger than the plastic indentation rate of 0.2 nm/h at the same time. This confirms that we are measuring a water assisted indentation process, and that ordinary plastic deformation has a negligible effect on our results.

To determine whether the precipitation rate or a nucleation barrier might cause the slowing down of the process, we have varied the amount of brine at the gold-sodium chloride contacts from 10^{-6} down to the amount of water adsorbed on the sodium chloride surface at a relative air humidity of 50%. A 10-μm indentation corresponds to a dissolved NaCl mass of $\approx 10^{-5}$ g. In 10 μl of saturated brine there is 3×10^{-3} g of NaCl. In this case, the dissolved mass will change the concentration by 0.3% if no NaCl is precipitated. In comparison, the solubility changes by 0.14% when the pressure changes from 0.1 to 4 MPa [28]. If the ''driving force'' for dissolution is expressed as the difference in solubility between the water at the contact (at 4 MPa) and at the free surface (at 0.1 MPa), it can be concluded that for the larger brine volumes the indentation by PSC may have progressed by several micrometers, even if there is no precipitation. For the system with adsorbed water only, there would be less than 1-nm indentation if there was no precipitation. If the rate of the measured indentation process was in any way limited by precipitation, large differences between the experiments would be expected. On the contrary, the data are described by extreme invariance to the brine volume, and we conclude that the process is not precipitation controlled.

The dissolution and precipitation kinetics of aqueous NaCl are very rapid at room temperature, $k_{\mathrm{diss}}=k_{\mathrm{prec}}=0.015$ mol/m^{2}s. For any of the models described above, PSC has been shown to be limited by diffusion when [31]

$$U=\frac{k_{\mathrm{diss}}d_i^2}{\Delta D c_{\mathrm{eq}}}>0.001, \tag{4}$$

where $c_{\mathrm{eq}}=5.4\times 10^3$ mol/m^3 is the equilibrium concentration [28]. In the FF and IC models, $d_i\sim 10^{-5}$ m is the width of the gold wires and 10^{-19} m^3/s$<\Delta D<10^{-15}$ m^3/s. In the IFF model, $d_i\sim 10^{-6}$ m is taken to be the width of the structures shown in Fig. 9 and 10^{-19} m^3/s$<\Delta D<10^{-15}$ m^3/s. Consequently, $10^{-2}<U<10^2$, and whichever model is used, this clearly indicates that the process is limited by diffusion of solutes out of the contact region. If the indentation rate was dissolution rate limited, then the indentation rate would be given by

$$\frac{\partial z}{\partial t}=\frac{k_{\mathrm{diss}}}{\rho}\left(1-\frac{K_{\mathrm{eq}}(p=0.1\ \mathrm{MPa})}{K_{\mathrm{eq}}(p=4\ \mathrm{MPa})}\right)=2\times 10^{-7}\ \mathrm{m/h}, \tag{5}$$

where ρ is the density of the solid. This is one to four orders of magnitude larger than the indentation rates measured in the experiments.

In order to test the effects of microstructural features in the crystals, we used both natural samples (from Windsor, Ontario, Canada delivered by Ward's Natural Science Establishment Inc., Rochester, NY, U.S.A.) and synthetic samples (delivered, polished by Pi-Kem, Shropshire, England) and we have used ground (1200–4000 mesh grinding paper with liquid paraffin lubricant, both from Struers A/S, Rodovre, Denmark), polished (using a suspension of 1-μm diamonds from Struers dispersed in dry hexadecane) and cleaved surfaces. The ground surfaces had scratch marks (up to 3 μm wide and deep) from the grinding paper such as those in Fig. 7. The polished surfaces had only suboptical scratches, with a width of less than 1 μm. The cleaved surfaces have no scratch marks, only atomically flat plateaus and steps of up to 3 μm between plateaus. The dislocation densities in the bulk and near the surfaces are assumed to vary between these samples. The use of flattened gold wires as indentors contributes to ''averaging'' over a large area ($\approx 5\times 10^{-7}$ m^2) of each crystal surface, while keeping the transport distance for dissolved material small (15–25 μm). The averaging ensures that the process is representative of each type of surface. The conformity of the indentation curves, irrespective of the surface treatment or sample provenance, indicates that the PSC process is not controlled by the distribution of preexisting dislocations in the material. This is not in conflict with earlier observations of dislocation density controlling PSC [24], because in that case the control acted through the process of ''healing,'' which is not possible in our experiment (because we use gold indentors instead of two crystals of the same material).

C. Structured contacts

After the indentation experiments by PSC, the salt crystal was quickly removed from the sample holder. It was flushed with a jet of hexane for a minute to remove brine and thus avoid crystal growth after the end of the experiment. The surface of the crystal was photographed through a microscope and the images were compared to photographs taken before the experiment. Invariably, the grooves left by indentation of the gold wires had a shell-like or island-channel-like structure such as that shown in Fig. 9. After some of the experiments were completed, we also used a white light interferometer to obtain a three-dimensional image of the surface. It can be seen in Fig. 9 that there are plateaus of linear dimension 2–6 μm with shallow channels (<1 μm) and deep pits (≈ 3 μm) in between. The structure was slightly dependent on the original surface treatment of the crystal and on the duration of the experiment.

D. Effects of temperature variations

During one of the 400-h-long experiments in which gold wires penetrated into NaCl by PSC, the effects of temperature variations were investigated. For 5 h the temperature was varied sinusoidally (using the Peltier element) with an amplitude of 0.1 K and a period of 30 min. Such a variation

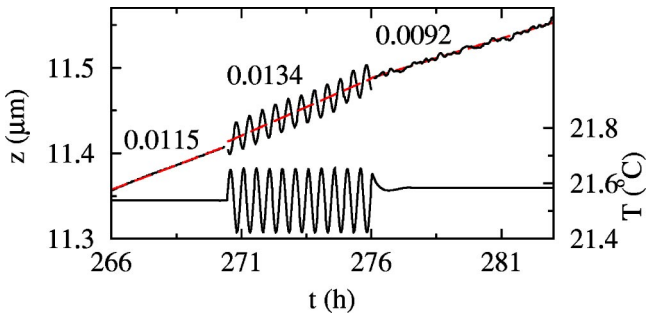

FIG. 10. Effect of temperature variation on indentation rate. A 16 h interval of a long experiment in which gold wires indented NaCl single crystal. For 5 h the temperature was varied sinusoidally with an amplitude of 0.1 K. Lower curve: measured temperature. Upper curve: measured indentation. Inset numbers are indentation rates in μm/h for the periods before, during, and after temperature variation.

of the temperature is typical if a simple water bath is used for temperature control. Figure 10 shows the temperature and indentation curves for this experiment. The steady slope of the indentation curve is due to irreversible indentation, while the sinusoidal variations are due to (reversible) thermal dilatation. Before the temperature variation was started the indentation rate was 0.0115 μm/h, and after the temperature variation was stopped the rate was 0.0092 μm/h. Without any temperature variation the indentation rate would have been $\approx(0.0115+0.0092)/2=0.0104$ μm/h. The indentation rate measured, while the temperature was varied, was 0.0134 μm/h (30% higher).

It was shown above that PSC *at constant temperature* is diffusion limited. The change in diffusion coefficient of aqueous NaCl due to a temperature change of 0.1 K is 0.3% [32]. It is clear that this cannot explain the measured rate change. A possible interpretation is that the 30% increase in indentation rate is an effect of varying the saturation concentration which results in an additional driving force for indentation: as the temperature rises it drives dissolution all over the crystal, contact and free surface areas alike, and as the temperature falls it drives precipitation on the free surface areas only. A temperature increase of 0.1 K causes a change in NaCl solubility of 0.004% which should be compared to the 0.14% difference in solubility between the liquid in the contacts and in the bulk.

The increase in indentation rate clearly shows the importance of good temperature control during experiments on systems with small driving forces, such as PSC. Small temperature changes can easily create driving forces larger than those associated with the process of interest.

E. Effects of normal stress variations

Figure 11 shows the response of the PSC process to sudden increase in normal stress. This experiment was performed with the single capacitance dilatometer. The only change made to the apparatus is that the force on the indentors giving the normal stresses was applied with a gas filled bellows instead of dead weights. The gas pressure was controlled by heating the gas in a chamber connected to the

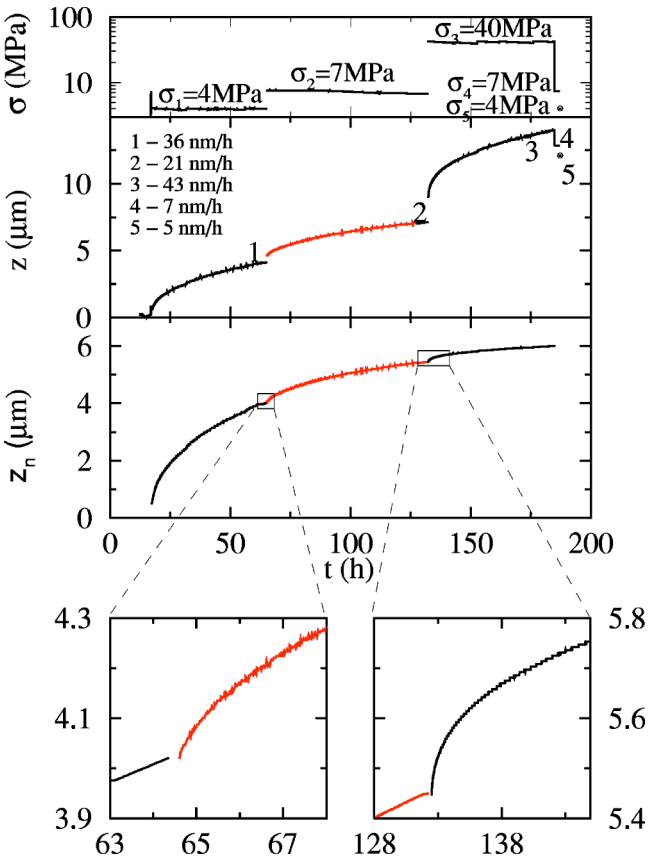

FIG. 11. Stepping of normal stress. Top: Sequence of normal stresses applied by gold wire indentors on the sodium chloride surface. Middle: Measured response (elastic compression and indentation by PSC) to normal stress sequence. Bottom and blowups: Normalized indentation z_n [see Eq. (6)].

bellows and measuring the gas pressure. In this experiment, we stepped the contact stress from ≈0.1 MPa in a sequence: (4, 7, 40, 7, 4) MPa. The response, z, measured by the dilatometer includes both the reversible elastic compression (of the sample, indentor, and piston) and the irreversible indentation by PSC. The elastic response is effectively instantaneous and is seen as open gaps in the curve. One observes that after each stress step the indentation rate increases suddenly and then decreases. Here, we observe in addition that this behavior does not only happen when indentors are brought in contact with the dissolving crystal for the first time, but it starts anew each time the stress is increased.

Simple thermodynamic considerations of the driving force for PSC predict that the indentation rate is proportional to normal stress. In order to better quantify the time-dependent effect of stress increase, we also display the measured data corrected for elastic compaction and normalized to 4 MPa normal stress:

$$z_n=(z-z_0)\frac{\sigma}{\sigma_1}-\Delta z_{elast}, \tag{6}$$

where z_0 is the measured height right after the stress was increased, σ is the new stress, $\sigma_1=4$ MPa, and Δz_{elast} is the elastic compaction. In the lower graph of Fig. 11 one observes the continuous indentation curve, much resembling indentation curves with constant stress. On closer inspection it is clear, however, that there is a marked increase in indentation rate at the onset of a stress increase even when the data has been normalized for the normal stress. In other words, it is not only the thermodynamic variable normal stress that affects the rate, but also the history, the time elapsed after the application of this stress.

One may counter that the indentation rate may, for some unknown reason, have a different dependence on normal stress, i.e., $\partial z/\partial t\sim\sigma^a$, $a\neq 1$. Applying larger powers, a, to the data one may obtain a local continous slope in the corrected experimental curve, but on a larger scale the curve looks discontinous.

The question remains whether the history dependence is some simple transient effect. When stress is increased, following the normal, thermodynamic treatment of PSC [1,7,8], one expects the solubility of sodium chloride in water to increase at the contacts. One might think that the system stays in a transient state until the contact region reaches the new state of local equilibrium. If this is the case, the same transient mechanism will cause the PSC to halt (or reverse) due to local supersaturation when stress is released. There is, however, no evidence of a transient phase in our data when the normal stress is stepped down from 40 MPa to 7 MPa and further to 4 MPa.

The observed increase in PSC rate after the increase in normal stress is therefore an irreversible, nonthermodynamic, time-dependent effect. It appears that the sudden increase of normal stress reactivates the unknown process that leads to the aging of the PSC process.

We have also performed experiments varying the normal stress sinusoidally. We have tried to vary the amplitude and frequency of the normal stress perturbations in order to gain further insight into the problem. It has proven extremely difficult to obtain good data with our single capacitance dilatometer. This is due to the large elastic response with respect to the subtle effects of PSC. The other problem is that our setup requires forces that are small compared to the stiffness of the bellows. However, we have obtained some interesting results displayed in Fig. 12. At the end of a long experiment with constant normal stress of 11.2 MPa, we applied a normal stress varying sinusoidally with an amplitude of 2 MPa and a period of 8.3 h. The middle graph in Fig. 12 shows the measured elastic and indentation response. We have not subtracted out the elastic response to show how large it is compared to the changes in PSC response. We have made a simple linear fit, $\hat{z}$, to the data, z, before the stress was varied:

$$\hat{z}=a+bt, \tag{7}$$

where a and b are fitting parameters and $t\in[450,485]$ h is the time. The bottom plot in Fig. 12 shows the data $z-\hat{z}$. Because of the strain hardening process $z-\hat{z}$ for $t<485$ h is curved around zero. If the PSC process was unaffected by the stress changes at $t>485$ h, the curve $z-\hat{z}$ would continue ever more negative due to the strain hardening. One

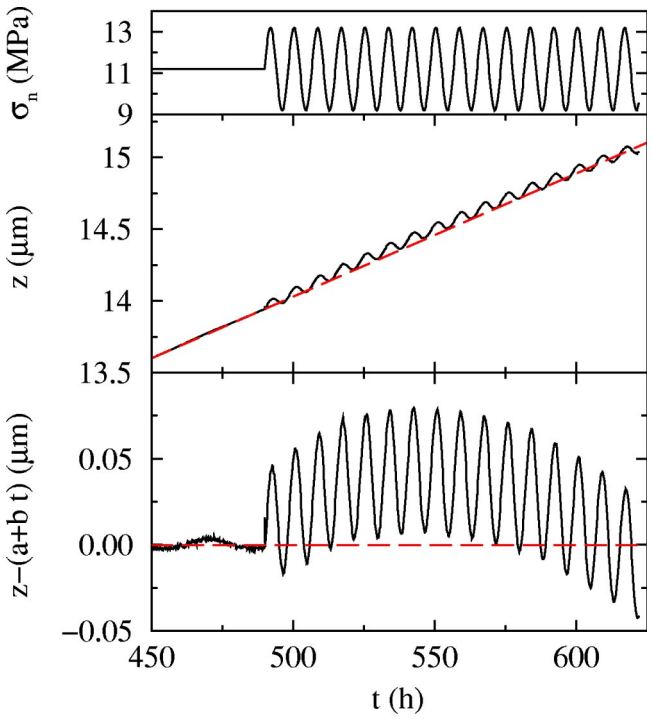

FIG. 12. Increased dissolution rate due to periodic normal stress variations. Top: Normal stress applied by gold wire indentors on the sodium chloride surface. Middle: Measured response (elastic compression and indentation by PSC) to normal stress sequence and straight line fit to constant stress response. Bottom: Measured response subtracted straight line fit.

observes, however, that at $t>450$ h the mean of the curve $z-\hat{z}$ goes positive. Thus, the sinusoidal normal stress variation speeds up the PSC process even though the mean stress is the same as before.

The differential dilatometer has been used to study the short time response to stepping of the normal stress. Figure 13 shows indentation of the tripod into sodium chloride at 0.4 MPa normal stress and a sudden increase in normal stress to 0.8 MPa at $t_0=25.391$ h. Due to the stability of the design, we obtain reliable data only a few seconds after increasing the dead weight load on the tripod. The bottom curve in Fig. 13 shows the indentation after the stress increase, $z-z_0$, as a function of time since the stress increase, $t-t_0$, in a log-log plot. The response starts off with a slope of 1/3 and increasing slightly after 10 h as the ''original creep curve'' (for 0.4 MPa) becomes relatively important.

In another experiment, we stepped the normal stress up and down several times. Figure 4 of Ref. [26] shows the applied variations in normal stress and the measured response. This experiment had larger problems with instability in the electronic circuit. It is, however, to some extent possible to separate the instabilities from the response to the normal stress. One observes that each time the stress is increased from 0.4 MPa to 0.8 or 1.2 MPa, the indentation starts rapidly and slows down again as in all the other experiments. In Fig. 3 of Ref. [26], we plot all the indentations $\Delta z=z-z_0$ for stress changes of 0.4–0.8 MPa together with the long time response at constant stress. The latter creep

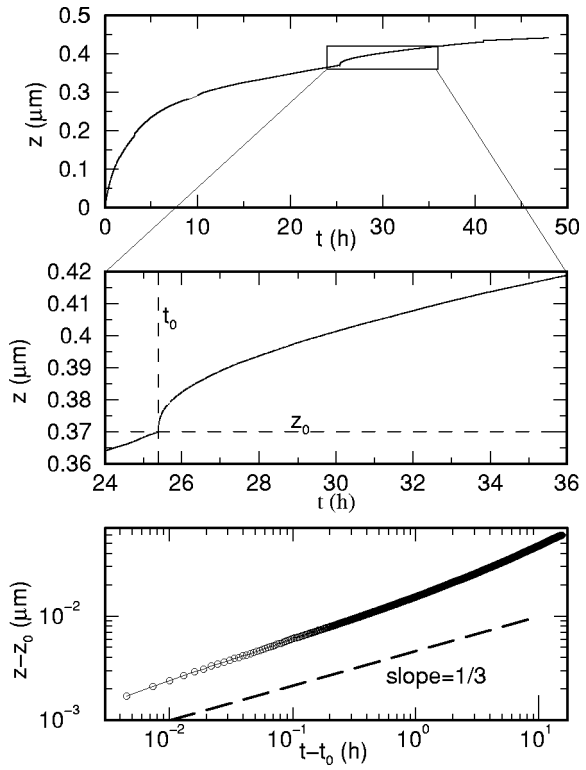

FIG. 13. Response to stepping of normal stress in differential dilatometer. Top curve shows 50 h indentation of a glass tripod into sodium chloride at 0.4 MPa normal stress and a sudden increase in normal stress to 0.8 MPa at $t_0=25.391$ h. The middle plot shows an enlargement of the response to the change in normal stress. Because the differential dilatometer was well balanced in this experiment and gave stable readings after 5 s, we plot the response to the stress increase in log log as well.

curves are in the asymptotic regime for $\Delta t>10$ h. One observes that the creep a short time after a stress increase has the same time dependence, $\Delta z \propto t^{1/3}$, as the long time behavior of the creep at constant stress.

F. Precipitation of pressure dissolved material

PSC requires dissolution, transport, and precipitation. To verify that the experimental observations are due to PSC, it is important to identify both the dissolved and the precipitated mass. This was quite difficult in our experiments because the mass dissolved by three gold wires would form a very thin layer if it was distributed uniformly over the large surface surrounding the indentors. Depending on the surface treatment, most often the precipitating salt did crystallize in very thin layers on the exposed surface. This made the precipitate impossible to distinguish from the original salt even when blue NaCl (nonstoichiometric NaCl with an excess of interstitial Na) was used. In some instances, when the original NaCl surface was scratched or damaged in other ways, the precipitating NaCl did not form a new layer on the existing crystal. Instead, the precipitate nucleated and grew as new crystals on the surface. Figure 14 shows micrographs from an experiment using a stainless steel grid as the indentor. The reason for using a grid is to have many small indentors to

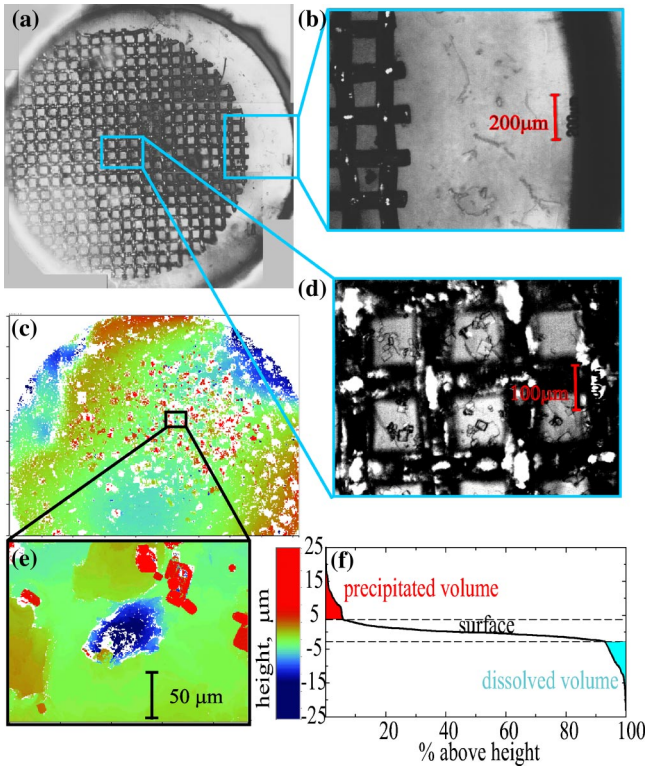

FIG. 14. Precipitation of pressure dissolved material. (a) Optical micrograph taken through the bottom window of the sample cell at the end of an experiment, before the system is perturbed. The image shows the wire mesh used as the indentor with a salt crystal on top. (b) Details of the outer part of wire mesh indentor showing no precipitated crystals. (d) Details of the middle of the indentor showing wire mesh and precipitated crystals on the original single crystal surface. (c) White light interferogram of the crystal in (a) after it has been removed from the sample holder. (e) Details from (c) showing a pressure dissolved pit and precipitated crystals. (f) Height data from (e) plotted as height vs percent of surface above this height, showing that 5% of the surface is precipitated crystals and 5% of the surface is pressure dissolved. The colored areas indicate the volumes dissolved and precipitated.

produce a larger mass that will precipitate. The top pictures (a), (b), and (d) were taken *in situ* looking upwards through the sapphire window at the bottom of the sample holder. At the end of the experiment, the sample holder was quickly removed from the temperature controlled environment and put on top of an inverted microscope. Salt crystals were observed to be sitting on top of the stainless steel grid that had been indenting the salt crystal for 5 weeks by PSC. The closeups show that there is also a large amount of secondary salt crystal growth on the salt surface between the wires of the grid. Away from the grid (away from the points of dissolution) almost no secondary salt crystals were observed. The bottom pictures [(c) and (e)] in Fig. 14 show micrographs recorded with a white light interferometer (WLI) after the salt crystal was removed from the sample holder. The WLI records height information over the entire imaged surface. The distribution of secondary salt crystals was found to be the same as that in the *in situ* micrographs. The observed length scale of mass transport from source to secondary crystals is of the order of 100 μm.

To obtain a rough estimate of the transport length scale, diffusion from a constant concentration source at the origin is described by the one-dimensional equation

$$\frac{\partial c}{\partial t} = D\frac{\partial^2 c}{\partial x^2} - \frac{k_{\mathrm{prec}}}{l_z}(1 - c/c_{eq}), \tag{8}$$

where c is the concentration, x is the position along the crystal surface, k_{prec} is the precipitation kinetic coefficient, l_z is the thickness of the fluid layer above the free crystal surface, and c_{eq} is the equilibrium concentration. The last term represents precipitation at the crystal surface. By expressing the one-dimensional diffusion equation in terms of the new variables $c' = (c/c_{\mathrm{eq}} - 1)$ and $x' = x/l_x$, where $l_x = \sqrt{D l_z c_{\mathrm{eq}}/k_{\mathrm{prec}}}$, and assuming steady state conditions, the equation

$$\frac{\partial^2 c'}{\partial x'^2} - c'^2 = 0 \tag{9}$$

is obtained. The solution to this equation is a simple exponential decay with a characteristic length of $l_x = \sqrt{D l_z c_{eq}/k_{\mathrm{prec}}} = 4 \times 10^{-8}$ m. The one-dimensional model is valid only in the limit $l_x \gg l_z$, and here it is used only to show that due to the rapid precipitation kinetics (large k_{prec}) $l_x \leqslant 1$ μm. The precipitate grows as secondary crystals and does not form a layer on the existing crystal because of surface damage. This causes effectively a nucleation barrier that modifies the simple precipitation model in Eq. (9) and thus explains the observation of crystals at $l_x > 10$ μm in this experiment.

For an area of linear dimension much larger than l_x, the mass dissolved should equal the mass precipitated. Figure 14(e) shows a high-resolution WLI image of the surface with secondary crystals surrounding a pit formed by pressure dissolution. Figure 14(f) displays the load bearing ratio of this region. This shows that the original surface occupies 87% of the total area, and that 6% of the area is above the original surface and 7% is below the original surface. The colored areas in Fig. 14(f) correspond to the precipitated and dissolved volumes (masses) and are observed to be roughly equal as expected.

As shown above, good temperature control is essential to avoid other driving forces for dissolution and precipitation. If the temperature varies and the fluid volume is large, the mass of precipitate from temperature variations can easily be larger than that from PSC. However, there is an important difference in the spatial distribution of the precipitate. In both cases, the precipitate will be close to the source. For PSC, most of the precipitate will be close to the indentor and for temperature variations, most of the precipitate will close to the large fluid volumes. The distribution of mass in our experiment demonstrates that PSC is the dominant process.

IV. DISCUSSION

We have established that the indentation curves presented in Fig. 8 arise from a PSC process in which material is dissolved at the gold-sodium chloride contacts and transported

to the free surface, where it is precipitated in the proximity of the indentor. We have shown that with the high degree of temperature control our results are negligibly influenced by temperature variations. The indentation rates are not controlled by either precipitation rates or the density of preexisting dislocations in the material, and ordinary plastic deformation is negligible. According to any of the existing models of PSC, the rate controlling step is diffusion. Because of the high precision and stability of our instrument, we have obtained data with unprecedented precision and repeatability that lends itself to quantitative comparison with proposed models of PSC.

The normal force F on the indentors is kept constant in our experiment. The only macroscopic parameter varying in time during the experiment is therefore the contact width d, which varies with indentation z (see Fig. 3). We wish to explore whether this can explain the observed slowing down of the PSC process. The normal stress at the contacts vary as $\sigma_n \propto F/d$, and according to Eq. (2)

$$\frac{\partial z}{\partial t} \propto \frac{\Delta D F}{d^3}. \tag{10}$$

In Fig. 8, we show a simple model for the flattening of the gold wires: The volume displaced from the flattened part is added to the sides described by circular arcs defined by the parameters d_0 and r_2. The width of the salt-gold wire contact is then expressed by

$$d(z) = d_0 + \sqrt{r_2^2 - (h-z)^2} \tag{11}$$

(see Fig. 8), where $d_0 = 6.49\ \mu$m, $r_2 = 21.7\ \mu$m, and $h = 20\ \mu$m. Inserting this simple model, $d(z)$, in the indentation rate equation (10)

$$t(z) = A_i + B_i \int d(z)^3 dz, \tag{12}$$

where A_i and B_i are constants, we can obtain the strain-time curves $z(t)$ corresponding to model (11). The model strain-time curves $z(t)$ can be fit to the experimental data by adjusting the parameters A_i and B_i. We have already shown that after 10 h the flat part of the gold wires are in contact with the sodium chloride crystals along their entire lengths. In some regions, the gold wires have just started to indent the sodium chloride surface,while in other regions they have penetrated further (up to 7.8 μm in one experiment). We will therefore require that the model strain-time curves coincide with the experimental data at this time: $z_{\mathrm{mod}}(t=10\ \mathrm{h}) = z_{\mathrm{exp}}(t=10\ \mathrm{h})$. Requiring the correct slope at 10 h, $\partial z/\partial t_{\mathrm{mod}}(t=10\ \mathrm{h}) = \partial z/\partial t_{\mathrm{exp}}(t=10\ \mathrm{h})$, gives the parameter set A_2 and B_2 with the resulting curve represented by long dashed lines in Fig. 8. Alternatively, if the model is matched to the data at long times, $z_{\mathrm{mod}}(t=370\ \mathrm{h}) = z_{\mathrm{exp}}(t=370\ \mathrm{h})$, the dot-dashed curve shown in Fig. 8 is obtained. Both curves clearly deviate from the experimental data. The slopes of the curves are even further off the mark, the long dashed curve has a slope at 300 h of 28 nm/h, which is four times larger than the slope of the experimental curves $\partial z/\partial t(t=200) = 7$ nm/h. The second curve starts out with a slope which is 2.5 times smaller and ends up with a slope $\partial z/\partial t(t=200) = 18$ nm/h which is 2.5 times larger than the slope of the curves obtained from the experimental data. Since the standard deviation of the experimental slopes at 200 h is only 9%, it may be concluded that the model expressed by Eq. (10) is incapable of explaining the time dependence of the experimental data. In addition, we note that the time-dependent creep $z(t)$ following stress increase shows the same time dependence, $z(t) \propto t^{1/3}$, for both gold wire indentors (see Fig. 11 and long time indentation curves in Fig. 3 in Ref. [26]) and glass cylinder tripod indentors (see Fig. 13 and short time indentation curves in Fig. 3 in Ref. [26]). The glass cylinder indentors have no change in macroscopic contact area after an initial indentation of 2 μm (see Fig. 5).

Clearly there is some time-dependent process involved that makes the indentation slow down faster than changes in macroscopic parameters can account for. We have recently reported measurements of the structure of the interface between the indentor and the NaCl undergoing PSC [26]. We find that the mean contact size d_c (in Fig. 1 or λ in Ref. [26]) increases with time as $d_c \sim t^{1/3}$ (see Fig. 3 in Ref. [26]). Assuming the fluid film model is valid at the contact scale [i.e., Eq. (2) with $d = d_c(t)$], one finds that

$$\frac{\partial z}{\partial t} \propto \frac{\Delta_c D_c \sigma_n}{d_c(t)^2} \propto t^{-2/3} \Rightarrow z(t) \propto t^{1/3}, \tag{13}$$

which is exactly the time evolution we report here for the indentation. The evolution of the contact region morphology can be interpreted as a spinodal dewetting process [26].

V. CONCLUSIONS

Two instruments with high precision and stability have been developed for measurement of PSC. The indentation by PSC of gold wires or glass cylinders into sodium chloride has been measured with unprecedented precision and repeatability. We have established that the measured indentation curves are the result of a PSC process in which material is dissolved at the indentor-sodium chloride contacts and transported to the free surface where it is precipitated in the proximity of the indentor. It has been demonstrated that our results are negligibly influenced by temperature variations. The indentation rates are not controlled by either precipitation rates or the density of preexisting dislocations in the material, ordinary plastic deformation is negligible and we conclude that the indentation rates must be diffusion controlled. The high precision and accuracy of our measurements has enabled us to discover a strain hardening effect that is explained by a new model of PSC with time-dependent contact sizes.

ACKNOWLEDGMENTS

The project had been supported by the Norwegian Research Council through the Fluid Rock Interaction Strategic University Program (Grant No. 113354-420 and by the Centre of Advanced Study at the Norwegian Academy of Sciences).

[1] P.K. Weyl, J. Geophys. Res. **69**, 2001 (1959).
[2] M.T. Heald, J. Geol. Chicago **14**, 16 (1956).
[3] S. Schwartz and B. Stöckhert, Tectonophysics **255**, 203 (1996).
[4] F. Renard, J.P. Gratier, and B. Jamtveit, J. Struct. Geol. **22**, 1395 (2000).
[5] S.A. Miller, Y. Ben-Zion, and J.P. Burg, J. Geophys. Res., [Planets] **104**, 10 621 (1999).
[6] R. Raj, J. Geophys. Res. B **87**, 4731 (1982).
[7] M.S. Paterson, Rev. Geophys. Space Phys. **11**, 355 (1973).
[8] R. Raj and C.K. Chyung, Acta Metall. **29**, 159 (1981).
[9] D.K. Dysthe, F. Renard, F. Porcheron, and B. Rousseau, Geophys. Res. Lett. **29**, 1109 (2002).
[10] S.W.J. den Brok, Geology **26**, 915 (1998).
[11] A.J. Gratz, Geology **19**, 901 (1991).
[12] D. Gal, A. Nur, and E. Aharonov, Geophys. Res. Lett. **25**, 1237 (1998).
[13] J. Ghoussoub and Y.M. Leroy, J. Mech. Phys. Solids **49**, 2385 (2001).
[14] F. Renard, Ph.D. thesis, University Joseph Fourier, Grenoble, 1997.
[15] F. Renard *et al.*, Geophys. Res. Lett. **28**, 1295 (2001).
[16] E.S. Sprunt and A. Nur, J. Geophys. Res. **82**, 3013 (1977).
[17] S.W.J. den Brok and J. Morel, Geophys. Res. Lett. **28**, 603 (2001).
[18] R. Tada and R. Siever, Geochim. Cosmochim. Acta **50**, 29 (1986).
[19] C.J. Spiers *et al.*, in *Deformation Mechanisms, Rheology and Tectonics*, edited by R.J. Knipe and E.H. Rutter, Geological Society Special Publication, Vol. 54 (The Geological Society, London, 1990), pp. 215–227.
[20] S.W.J. den Brok and C.J. Spiers, J. Geol. Soc. (London) **148**, 541 (1991).
[21] C.J. Spiers and R.H. Brzesowsky, Seventh Symposium on Salt **I**, 83 (1993).
[22] P.M. Schutjens and C.S. Spiers, Oil Gas Sci. Technol. **54**, 729 (1999).
[23] S.H. Hickman and B. Evans, J. Geol. Soc. (London) **148**, 549 (1991).
[24] S.H. Hickman and B. Evans, in *Fault Mechanics and Transport Properties of Rocks*, edited by B. Evans and T.F. Wong (Academic, San Diego, 1992), pp. 253–280.
[25] T.H. Johansen, J. Feder, and T. Jøssang, Rev. Sci. Instrum. **57**, 1168 (1986).
[26] D.K. Dysthe *et al.*, Phys. Rev. Lett. **89**, 246102 (2002).
[27] R.V. Jones, *Instruments and Experiences* (Wiley, New York, 1988).
[28] *Soldium Chloride: The Production and Properties of Salt and Brine*, edited by D.W. Kaufmann, American Chemical Society Monograph Series 145 (Reinhold, New York, 1960).
[29] S.W.J. den Brok, M. Zahid, and C.W. Passchier, Tectonophysics **307**, 297 (1999).
[30] A.H. Cottrell, *Dislocations and Plastic Flow in Crystals* (Clarendon Press, Oxford, 1953).
[31] E. Gundersen *et al.*, in *Deformation Mechanisms, Rheology and Tectonics: Current Status and Future Perspectives*, edited by S. de Meer *et al.*, Geological Society Special Publication, Vol. 200 (The Geological Society, London, 2002), pp. 41–56.
[32] R. Castillo and C. Garza, Int. J. Thermophys. **14**, 1145 (1993).